Analytic Centre Based Tension Distribution for Cable-Driven Platforms (CDPs)

Vincenzo Di Paola, Alexandre Goldsztejn, Matteo Zoppi, Stéphane Caro

Analytic Centre Based Tension Distribution for Cable-Driven Platforms (CDPs)

Vincenzo Di Paola*
University of Genova - DIME, Genova, Italy
Nantes Université, École Centrale Nantes
CNRS, LS2N, UMR 6004
1, rue de la Noe, 44321 Nantes, France
Email: vincenzo.dipaola@edu.unige.it

Alexandre Goldsztejn
Nantes Université, École Centrale Nantes
CNRS, LS2N, UMR 6004
1, rue de la Noe, 44321 Nantes, France
Email: alexandre.goldsztejn@ls2n.fr

Matteo Zoppi
University of Genova - DIME, Genova, Italy
Email: matteo.zoppi@unige.it

Stéphane Caro
ASME Member
Nantes Université, École Centrale Nantes, CNRS
LS2N, UMR 6004, 1, rue de la Noe, 44321 Nantes, France
Email: stephane.caro@ls2n.fr

ABSTRACT

A redundant Cable-Driven Platform (CDP) is composed of m cables that exceed the Degree of Freedom (DOF) of the end-effector. The choice of tension along the cables admits infinite solutions. This paper proposes the use of the Analytic Centre to solve the tension distribution problem. Adopting this technique allows finding tensions far from the tension limits namely, *robust* as well as tension profiles continuous and differentiable in time. The continuity, differentiability and uniqueness of the solution is also proven. Moreover, the possibility of including non-linear constraints acting on the tensions (e.g. friction) is a further contribution. The computational time with the proposed approach is compared to the existing techniques to assess its real-time applicability. Finally, several simulations using several CDPRs' architectures are reported to demonstrate the method's capabilities.

1 INTRODUCTION

Cable-Driven Platform (CDP) encompasses a class of seemingly diverse robots that can actually be characterized by a unified mathematical model. Within this class of robots one can find the widely established *Cable-Driven Parallel Robots* [1] (CDPRs) and the newcomers *Aerial Cable Towed Systems* [2] (ACTSs) or a hybrid version between CDPRs and ACTSs also known as *Hybrid-ACTSs* [3]. The rapid development of CDPs is due to their inherent capabilities such as high tracking speed, large workspace, reconfigurability and modularity, which make them suitable for a vast category of applications such as crane-like

*Corresponding author.

applications [4, 5], rehabilitation [6, 7], filming [8], aerial load transportation to cover long distances [9, 10], post-disaster scenarios [11] and so on. Generally speaking, the presence of cables brings advantages such as reduced inertia and low cost while making them collaborative with humans due to their inherent flexibility. Despite the mentioned advantages, there is an added complexity in operating with cables. Indeed, guaranteeing cable tautness and smooth variations of the tension values during the execution of a task poses several problems. The management of cable tensions is still a topic of ongoing research. When the Degree of Redundancy DoR[1] ≥ 1 namely *redundant* CDPs are considered, infinitely many solutions to the tension distribution problem may exist. In this view, one chance of solving this problem is to formulate an optimisation problem and solve it iteratively. The 1-norm of the tension vector $\boldsymbol{\tau}$ is the protagonist of several previous works [12, 13, 14]. Linear Program (LP) are notable for their fast convergence, which makes them suitable for real-time applications. Though, the optimal point is always placed at the edge of the tension box and, between two iterations, it can jump from one edge of the polyhedron to the other, resulting in discontinuities between two successive solutions. The same can happen also with the ∞-norm [15], thus, to overcome this issue and guarantee continuity between solutions, the p-norm $1 < p < \infty$ can be used [16]. In fact, practically, a natural extension consists in using the 2-norm of the tension vector [17, 18] and in solving a Quadratic Program (QP) whose accessibility makes it popular. Even so, other solutions were explored for example, in [19, 20] the Dykstra alternating-projection algorithm is used to solve the minimum 2-norm tension distribution. Another alternative to tackle the tension distribution problem, ensuring continuity, takes the barycenter of the polyhedron as the optimal solution [21]. Evidently, the criteria are different and their choice depends on the assigned task. Indeed, for example, the 2-norm methods can guarantee reducing power consumption whereas barycenter is said to be *safe* since the solution is far from cable tension limits. Besides, the Improved-Closed Form method [22], built on its predecessor [23], tries to reduce the method complexity by maintaining real-time efficiency, generality w.r.t. the DoR and continuity of the tension profiles. Even so, these methods do not guarantee the convergence in the entire Wrench Feasible Workspace (WFW) [24]. In addition, since the Improved-Closed Form approach set outbound cable tensions to their maximum or minimum value, the smoothness of tension profiles can be compromised. Analogously, with the intention of maximising the applicability of the method within the WFW without degrading continuity and algorithm speed, in [25] they take their inspiration from [22] and develop the Improved Puncture Method. A strategy for tension distribution dealing with CDPRs operating beyond their WFW is also explored in [26]. Actually, many works were proposed to establish an opportune set of tensions to be used during the fulfilment of a given task. However, only one [27] introduces a versatile tension distribution algorithm, which allows computing several types of mentioned techniques. Nevertheless, the introduced algorithm can be applied only for CDPRs with, at most, $DoR = 2$. In this context, this paper aims to build on the Analytic Centre (AC) method. Indeed, thought this technique has been introduced in a short paper [28], several important peculiarities have been omitted. Hence, the contributions here are the following

1. a detailed review of the existing TDAs is given in Section 3. This allows both comparisons and understanding why the AC approach is indeed relevant;
2. the extension of the method to include non-linear constraints (e.g. friction) in the optimisation problem. Notice that, incorporating time-varying non-linear constraints to compute cable tensions increases the range of applicability of this TDA to other types of CDP as, for example, for the Mobile Cable-Driven Parallel Robots (MCDPRs) [29, 30, 31];
3. proof of the continuity and differentiability of cable tension profiles is presented taking into account, explicitly, the possibility of including non-linear constraints;
4. the main disadvantages and limitations are outlined as a completion analysis of the AC method.

[1] $DoR = m - n$ where m is the cable number and n stands for the *Degree of Freedom* (DoF) of the platform.

This paper is structured as follows: in Section 2 the CDP model and the main definitions necessary to state the tension distribution problem are recalled. A motivating example opens Section 3 followed by the definition of the Analytic Centre in Section 4. The continuity and differentiability are rigorously proven as well as the existence of a unique solution for the parametric optimization problem. Subsequently, Section 5 includes simulations with various CDPR architectures while Section 6 draws the conclusion and outlines future works.

2 CDP MODEL

In this section, the main equations and symbols necessary to describe the CDP are hereby reported. The static or dynamic equilibrium of a platform in the space, guided by m cables, is governed by the following equation

$$\mathbf{W}\boldsymbol{\tau} + \mathbf{w}_e = \mathbf{0}, \tag{1}$$

where, in general, $\mathbf{w}_e \in \mathbb{R}^6$ is the external wrench which also takes into account dynamical actions applied to the platform, $\boldsymbol{\tau} \in \mathbb{R}^m$ is the cable tensions vector, $\mathbf{W} \in \mathbb{R}^{6\times m}$ is the wrench matrix which is defined as

$$\mathbf{W} = \begin{pmatrix} \mathbf{u}_1 & \dots & \mathbf{u}_m \\ \mathbf{b}_1 \times \mathbf{u}_1 & \dots & \mathbf{b}_m \times \mathbf{u}_m \end{pmatrix}, \tag{2}$$

here $\mathbf{u}_i \in \mathbb{R}^3$ represents the ith cable direction unitary vector and $\mathbf{b}_i \in \mathbb{R}^3$ represents the ith attachment point on the platform. Thus, if $DoR \geq 1$, there exist infinite solutions of Eq.(1) grouped in the following set

$$\Sigma = \left\{ \boldsymbol{\tau} \,|\, \mathbf{W}\boldsymbol{\tau} + \mathbf{w}_e = \mathbf{0} \right\}. \tag{3}$$

However, to maintain the equilibrium of the platform the cable tension limits have to be taken into account. Hence, the m-dimensional convex hypercube Π, that defines the domain of the *feasible* tensions, is

$$\Pi = \left\{ \boldsymbol{\tau} \,|\, \mathbf{0} < \underline{\boldsymbol{\tau}} \leq \boldsymbol{\tau} \leq \overline{\boldsymbol{\tau}} \right\}, \tag{4}$$

where $\underline{\boldsymbol{\tau}}, \overline{\boldsymbol{\tau}} \in \mathbb{R}^{m,+}$ are positive tension vectors limits containing the ith lower and upper cable tension limits as components, which, without loss of generality, will be considered equal to each other, respectively. Consequently, the set of feasible solutions Γ satisfying both Eq.(1) and Eq.(4), is

$$\Gamma = \Sigma \cap \Pi. \tag{5}$$

This equation summarises the tension distribution problem: in fact, it consists in finding tensions that guarantee both the equilibrium of the platform and that do not exceed the lower and upper limits. Practically, the cable tensions can be computed as

$$\begin{aligned} \boldsymbol{\tau} &= -\mathbf{W}^{\dagger}\mathbf{w}_e + \mathbf{N}\boldsymbol{\lambda} \\ &= \boldsymbol{\tau}_p + \boldsymbol{\tau}_g, \end{aligned} \tag{6}$$

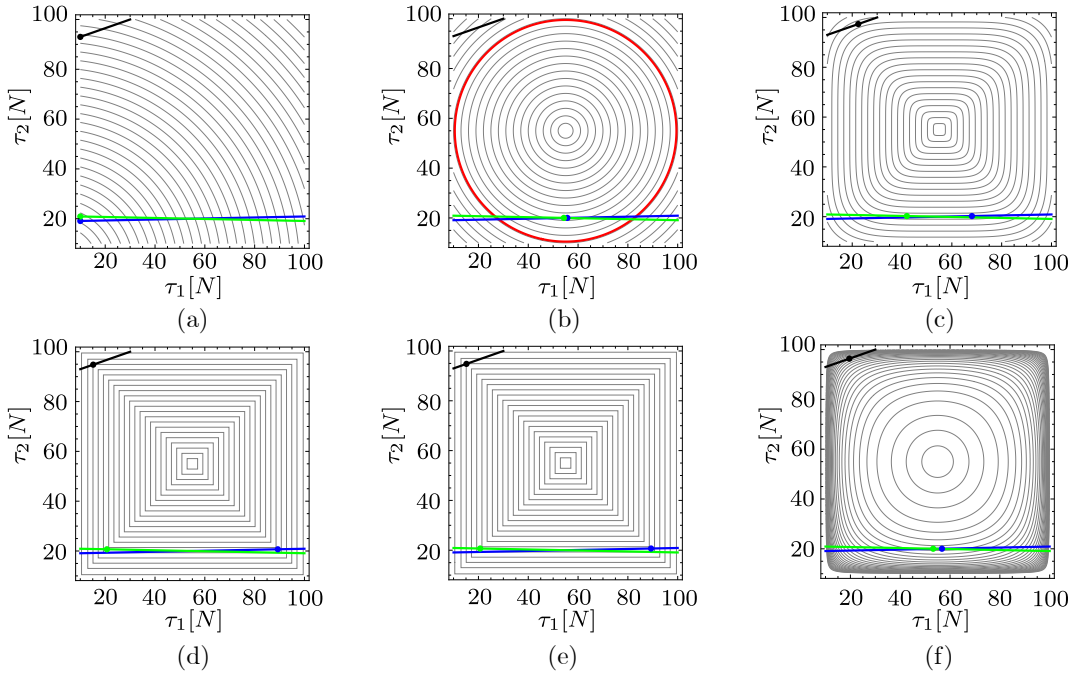

Fig. 1: Level-sets: (a) the 2-norm with respect to the origin $(0, 0)$, (b) the 2-norm with respect to the centre of Π, (c) the 5-norm within Π, (d) the ∞-norm within Π, (e) the distance to the closest boundary of Π and (f) the logarithmic barrier over Π. Three test cases are displayed in black, blue and green respectively. From the Lagrange optimality conditions, if a minimizer lies strictly inside the cable tension box, then the level-set of the cost function and the linear subspace $\mathbf{W}\boldsymbol{\tau} + \mathbf{w}_e = \mathbf{0}$ are tangent at this minimizer. Using generalized gradients, this tangency condition is satisfied at corners of non-smooth level-sets in the figures (d) and (e).

where $\mathbf{W}^\dagger = \mathbf{W}^T(\mathbf{W}\mathbf{W}^T)^{-1}$ is the Moore-Penrose pseudo-inverse matrix of $\mathbf{W}$, $\mathbf{N} \in \mathbb{R}^{m\times(m-n)}$ contains the vectors that span the kernel of $\mathbf{W}$, $\boldsymbol{\lambda} \in \mathbb{R}^{(m-n)}$ belongs to the polytope Λ in Eq.(7) and $\boldsymbol{\tau}_p$, $\boldsymbol{\tau}_g$ are the particular and general solution of Eq.(1), respectively. For sake of clarity, the definition of the convex polytope Λ is reported in

$$\Lambda := \{\boldsymbol{\lambda} \in \mathbb{R}^{(m-n)} \,|\, \underline{\boldsymbol{\tau}} \leq -\mathbf{W}^\dagger \mathbf{w}_e + \mathbf{N}\boldsymbol{\lambda} \leq \overline{\boldsymbol{\tau}}\}. \tag{7}$$

It turns out that, to cope with the cable intrinsic property, guaranteeing the controllability of the platform during the tasks, a natural way to deal with Eq.(6) consists in solving an optimization problem. So far, several approaches were presented in the literature. Therefore, a motivation and an overview of the context in which this contribution lies is given in the next section.

3 MOTIVATING EXAMPLE

3.1 Description

This section considers an academic example that consists in distributing two tensions $\boldsymbol{\tau} = (\tau_1, \tau_2)$ belonging to a box $\Pi = \{\boldsymbol{\tau} \,|\, \mathbf{0} < \mathbf{10} \leq \boldsymbol{\tau} \leq \mathbf{100}\}$ with corners $\underline{\boldsymbol{\tau}} = (10, 10)$ and $\overline{\boldsymbol{\tau}} = (100, 100)$. The level-sets of different tension distribution optimization problems are displayed in Figure 1. Tensions are required to satisfy the static equilibrium constraint $\mathbf{W}\boldsymbol{\tau} + \mathbf{w}_e = \mathbf{0}$ with $\mathbf{W} \in \mathbb{R}^{1\times2}$ and $\mathbf{w}_e \in \mathbb{R}^1$. Three

test cases are considered: the first takes $\mathbf{W} = (-7, 20)$ and $\mathbf{w}_e = (-1790)\, N$ and it is displayed in black in Figure 1. The second takes $\mathbf{W} = (-1, 50)$ and $\mathbf{w}_e = (-945)\, N$ and it is displayed in blue in Figure 1. The third takes $\mathbf{W} = (1, 50)$ and $\mathbf{w}_e = (-1055)\, N$ and it is displayed in green in Figure 1. The last two sets of data are very similar to each other, being representative of close poses or of the effect of uncertainties on a pose, and are presented to illustrate the sensitivity of the solution given by the Tension Distribution Algorithms (TDAs).

In all the cases, the barycenter of the feasible polytope Λ coincides with the midpoint of the two intersections between the line $\mathbf{W}\boldsymbol{\tau} + \mathbf{w}_e = \mathbf{0}$ and the borders of Π.

3.2 State-of-the-art optimization based TDAs

TDAs based on minimizing the 2-norm have been widely investigated and used. They rely on solving the linearly constrained quadratic problems:

$$\underset{\substack{\mathbf{W}\boldsymbol{\tau}+\mathbf{w}_e=\mathbf{0} \\ \boldsymbol{\tau}\in\Pi}}{\operatorname{argmin}} \|\boldsymbol{\tau}\|_2 \quad \text{and} \quad \underset{\mathbf{W}\boldsymbol{\tau}+\mathbf{w}_e=\mathbf{0}}{\operatorname{argmin}} \|\boldsymbol{\tau} - \hat{\boldsymbol{\tau}}\|_2 \tag{8}$$

with $\hat{\boldsymbol{\tau}} = \frac{1}{2}(\underline{\boldsymbol{\tau}} + \overline{\boldsymbol{\tau}})$ the midpoint of Π. The first allows minimizing the required energy to the actuators, hence it offers a limited stiffness. Furthermore, its minimizer often lies on the boundary of Π and is therefore not considered in the context of robust tension distribution. The level-sets of the cost function $\|\boldsymbol{\tau}\|_2$ and the corresponding minimizers are shown in Figure 1-(a). It is possible to see that green and blue tension vectors are close to each other, indicating a low sensitivity of the investigated TDA. Minimizing $\|\boldsymbol{\tau} - \hat{\boldsymbol{\tau}}\|_2$ is meant to compute tension vectors as close as possible to the centre of Π. It is therefore attracting for pursuing robust tension distribution. Using the 2-norm allows for a Closed Form solution of Eq.(8), see [23]. This Closed Form solution is additionally attractive because its computation requires only to evaluate the pseudo-inverse of $\mathbf{W}$. The green and blue solutions displayed in Figure 1-(b) are seen to be very close to each other, showing again a low sensitivity of this TDA.

Since the inequality constraints are not taken into account, the solution of the optimization problem can be outside Π while some feasible solution exists, and indeed the black solution is not visible in Figure 1-(b) because it is outside Π (see also Figure 2 in [23] for a more detailed discussion). This results in a reduced WFW coverage. A corrected version of the Closed Form formula, aiming at setting to the lower or upper limit cable tensions that exceed the boundaries, was introduced in [22], but with no sound of theoretical proof for the convergence and continuity. Furthermore, this adjusted Closed Form tension vector is meant to lie on the boundary of Π, hence not satisfactory with respect to robustness.

Remark 3.1. *Correcting the Closed Form formula (or directly) solving Eq.(8) with the inequality constraints $\boldsymbol{\tau} \in \Pi$ using a numerical solver has not been considered in the literature yet to the best of authors knowledge. Its numerical optimization is as complex as with $\hat{\boldsymbol{\tau}} = \mathbf{0}$, and is therefore also attractive. However, when the Closed Form solution is outside Π, the corrected constrained solution will lie on the Π boundary, hence not being satisfactory in terms of robustness.*

Remark 3.2. *Using p-norms, including $p = \infty$, was discussed in [32] while the case $p = 4$ was extensively discussed in [15] where a Closed Form solution is also given. The level-sets of the ∞-norm with respect to the centre of Π are shown in Figure 1-(d). The tangency condition (i.e. optimality) is satisfied when the linear subspace meets a corner of the level-set, as illustrated by the three solutions represented. Because the level-sets are straight lines, cases where the linear subspace $\mathbf{W}\boldsymbol{\tau} + \mathbf{w}_e = \mathbf{0}$ is parallel to the level-sets have an entire segment of solutions, and an infinitesimal change in the data of the problem will cause an*

abrupt transition to one or the other segment endpoints. This occurrence is illustrated on Figure 1-(d) by the high sensitivity of the blue and green neighbour problems, whose solutions are characterized by a large distance. Intermediate behaviors are obtained considering p-norms with $2 < p < \infty$: Figure 1-(c) shows the level-sets of the 5-norm. The black solution computed is now inside Π. There is no straight level sets anymore, but the presence of almost straight level-sets show a strong sensitivity as well, as illustrated by the large distance between the blue and green solutions.

With the aim of maximizing the robustness of the TDA, in [12] it was proposed to maximize the distance to the closest face of Π. This leads to the following optimization problem:

$$\underset{\substack{\mathbf{W}\boldsymbol{\tau}+\mathbf{w}_e=\mathbf{0}\\ \boldsymbol{\tau}\in\Pi}}{\operatorname{argmax}} \; d(\boldsymbol{\tau}), \tag{9}$$

where $d(\boldsymbol{\tau}) = \min\{\overline{\tau}-\tau_1, \tau_1-\underline{\tau}, \overline{\tau}-\tau_2, \tau_2-\underline{\tau}\}$ is the distance to the closest face of Π or, equivalently, the *robustness index*. This optimization problem is classically reformulated to an easy-to-solve Linear Program (LP). Figure 1-(e) shows the level-set of $d(\boldsymbol{\tau})$. In spite of its advantage in terms of robustness, this approach shows a very high sensitivity, illustrated by the large distance between the blue and green solutions. This happens when the linear subspace $\mathbf{W}\boldsymbol{\tau}+\mathbf{w}_e = \mathbf{0}$ is close to be parallel to an axis. Although, in practice, the exact time where the linear subspace is exactly parallel to an axis is in general not at a time-step where the optimization problem is solved, this leads to potentially discontinuous tension profiles, as detailed in [12].

Remark 3.3. *Figures 1-(d)(e) show a surprising coincidence between the level-sets of the ∞-norm with respect to the centre and the distance to the closest face. This coincidence leads to the same minimal and maximal tension vectors. As far as the authors know, this coincidence was not made explicit in this context, and actually holds, in general, when tension limits are independent of cables[2], i.e., $\underline{\tau}_i = \underline{\tau}_j = \underline{\tau}$ and $\overline{\tau}_i = \overline{\tau}_j = \overline{\tau}$. The distance to the closest face of Π is then*

$$d(\boldsymbol{\tau}) = \min\{\overline{\tau}-\tau_1, \tau_1-\underline{\tau}, \ldots, \overline{\tau}-\tau_m, \tau_m-\underline{\tau}\}. \tag{10}$$

In the following, the constraints $\mathbf{W}\boldsymbol{\tau}+\mathbf{w}_e = \mathbf{0}$ and $\underline{\boldsymbol{\tau}} \le \boldsymbol{\tau} \le \overline{\boldsymbol{\tau}}$ are implicit in the optimization problems to lighten the notation. Recall that $\operatorname{argmax} f = \operatorname{argmin} -f$ and that adding the radius $r = \frac{1}{2}(\overline{\tau}-\underline{\tau})$ to the cost function does not change its argument. Furthermore, the radius r and centre $\hat{\tau} = \frac{1}{2}(\overline{\tau}+\underline{\tau})$ are related by $\overline{\tau}-r = \hat{\tau}$ and $\underline{\tau}+r = \hat{\tau}$. Then, basic manipulations show that:

$$\begin{aligned}
&\operatorname{argmax} d(\boldsymbol{\tau}) = \operatorname{argmin}\big(-d(\boldsymbol{\tau})+r\big) && \text{(11a)}\\
&= \operatorname{argmin} \max\{\tau_1-\hat{\tau}, \hat{\tau}-\tau_1, \ldots, \tau_m-\hat{\tau}, \hat{\tau}-\tau_m\} && \text{(11b)}\\
&= \operatorname{argmin} \max\{|\tau_1-\hat{\tau}|, \ldots, |\tau_m-\hat{\tau}|\} && \text{(11c)}\\
&= \operatorname{argmin} \|\boldsymbol{\tau}-\hat{\boldsymbol{\tau}}\|_\infty. && \text{(11d)}
\end{aligned}$$

3.3 The Analytic Centre

A great advantage of the TDA corresponding to the distance to centre with 2-norm and no inequality constraints is that the absence of inequality constraints allows an efficient resolution. In this special case, a

[2] Both TDAs are not well defined in case of cable dependent tensions limits since the aim is to maximize the distance $d(\boldsymbol{\tau})$ from the boundaries $\overline{\tau}$ and $\underline{\tau}$.

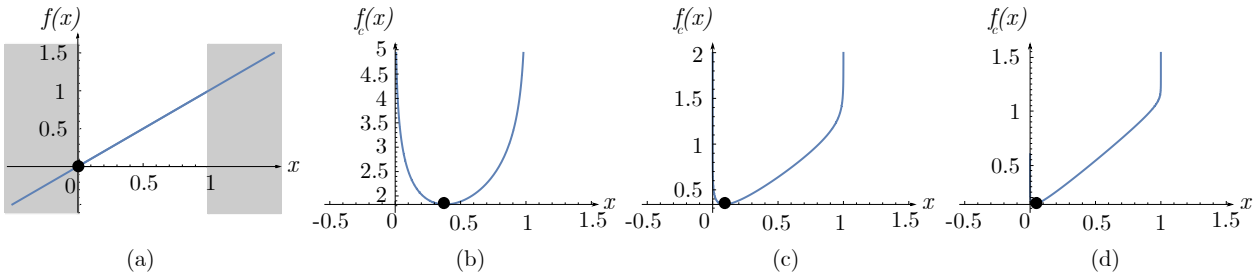

Fig. 2: Barrier function: (a) the cost function $f(x) = x$ subject to $g(x) = x(x-1) \leq 0$ represented by gray areas. Remaining graphics (b),(c) and (d): the unconstrained problem $f_c(x) = c\log(-x(x-1))$ with $c \in \{1, 0.1, 0.01\}$. One can observe that the unconstrained minimizer "dot" in the graphs converges toward the constrained minimizer as c converges to 0. In other words, using $\log(...)$ and tuning c allows to approximate the original problem with an underconstrained ones.

Closed Form solution is available but, in general, numerical optimization is easier and more efficient when only linear equality constraints are enforced: basically, inequality constraints require determining which inequality is active at minimizer, entailing more complex algorithms. One expedient in optimization foresees the usage of logarithmic barrier functions, which change inequality constrained minimization problems of $f(x)$, subject to inequality constraints $g_i(x) \leq 0$, to unconstrained minimization problems consisting in minimizing $f(x) - c\sum_i \log\big(-g_i(x)\big)$. In the context of inequality constrained optimization, the parameter c is meant to converge to zero during the resolution in order to reduce the impact of the barrier function on the objective, see Figure 2.

Remark 3.4. *The logarithmic barrier is preferred to other barrier functions like* $\frac{1}{g(x)}$ *or* $\frac{1}{g(x)^2}$ *because it is self-concordant, following a theory introduced in the late 80's by Nesterov and Nemirovski [33] which allows bounding the number of Newton iterations required to reach a prescribed accuracy on the minimum. Such a good convergence characterization of the numerical optimization is of critical importance for real time usage of the TDA.*

For a fixed value of the barrier coefficient c, the barrier actually attracts the solution inside the solution set. Hence, one aim of this paper is to use this property to enforce the robustness on the tension solution. This can be achieved considering the so-called Analytic Centre associated with the constraints $\boldsymbol{\tau} \in \Pi$ and $\mathbf{W}\boldsymbol{\tau} + \mathbf{w}_e = \mathbf{0}$, which is defined as:

$$\underset{\mathbf{W}\boldsymbol{\tau}+\mathbf{w}_e=\mathbf{0}}{\operatorname{argmin}} \ \phi(\boldsymbol{\tau}) \quad \text{with} \quad \phi(\boldsymbol{\tau}) = \sum_{i=1}^{2} -\log(\overline{\tau} - \tau_i) - \log(\tau_i - \underline{\tau}). \tag{12}$$

The Analytic Centre definition, as well as many properties and related methods of numerical optimization, can be found in [34, Sec.9.1]. As seen in Eq.(12), the logarithm barrier function enforces $\boldsymbol{\tau}$ to be strictly inside Π.

Remark 3.5. *In the framework of convex optimization, it is classical to consider the constraint* $\boldsymbol{\tau} \in \operatorname{int}(\Pi)$ *(i.e. interior of* Π*) implicit in Eq.(12) with* $\phi(\boldsymbol{\tau}) = +\infty$ *when logarithms are not defined. In particular, this emphasizes that optimization methods dedicated to problems with linear equality constraints and no inequality constraints are used to solve Eq.(12).*

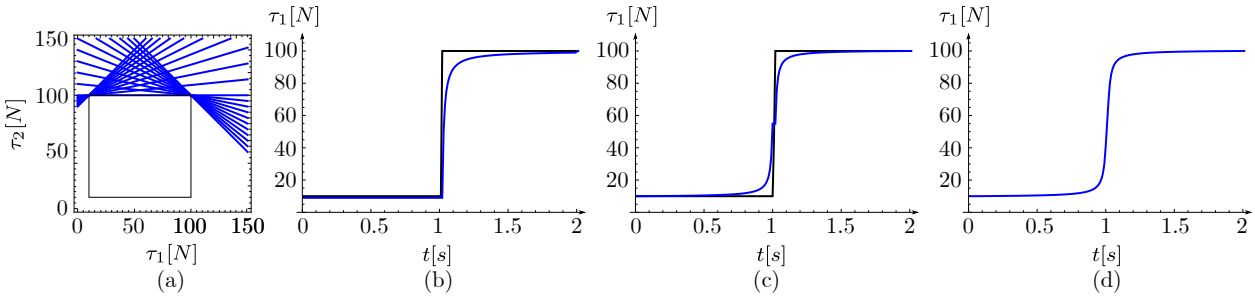

Fig. 3: Discontinuity example: (a) intersection of Π (tension box) with the time dependent linear constraint Eq.(1) which does not satisfy Slater's condition since it touches the boundary of Π. Remaining graphics: in black, the tension profile $\tau_1(t)$, for (b) the minimal 2-norm to the origin, (c) the barycenter and (d) the Analytic Centre. In blue, the same profile for a slightly enlarged Π. The idea is to illustrates the abrupt change in the tension profile at $t = 1s$ caused by the high sensitivity of TDAs near to the boundary of Π. Furthermore, this example shows the behaviour of the TDAs when the Slater's condition is not satisfied.

The level-sets of $\phi(\boldsymbol{\tau})$ are shown in Figure 1-(f). One can observe that the Analytic Centre optimization problem offers a much better compromise between the 2-norm to the centre and the ∞-norm to the centre of Π than the 5-norm does[3]: first, contrarily to the 2-norm to the centre and similarly to the ∞-distance to the centre of Π, the Analytic Centre is inside Π under the weak assumption[4] that the linear subspace $\mathbf{W}\boldsymbol{\tau} + \mathbf{w}_e = \mathbf{0}$ intersects the interior of Π, see the black solution for a typical case where the minimal 2-norm is outside Π while the analytic centre is inside. Second, the level sets are similar to circles in a neighborhood of the centre of Π, hence showing a low sensitivity in this area, as illustrated by the blue and green solutions in Figure 1-(f), which can be compared to the ones in Figure 1-(c), where the blue and green solutions are far away in the case of the 5-norm to the centre of Π.

Remark 3.6. *Every TDA must show a high sensitivity near the boundary of* Π. *This is illustrated with the minimal* 2*-norm and the barycenter by the following limit case: with the same* Π *as before, let* $\mathbf{W}(t) = (1-t, -1)$ *and* $\mathbf{w}_e = 100 + 45|1-t| - 55(1-t)$. *The time varying linear subspace* $\mathbf{W}(t)\boldsymbol{\tau} + \mathbf{w}_e(t) = \mathbf{0}$ *is displayed in Figure 3-(a). It intersects only the boundary of* Π, *hence not satisfying Slater's condition at any time. More precisely, one can observe that, for* $t < 1$, *the only feasible tension is* $\boldsymbol{\tau} = (10, 100)$, *therefore both TDAs in Figs. 3-(b)(c) will output this tension while, for* $t > 1$, *the only feasible tension is* $\boldsymbol{\tau} = (100, 100)$, *and, then, both TDAs will output this tension. For* $t = 1$, *the whole upper face of* Π *is feasible, so the minimal* 2*-norm is attained for* $\boldsymbol{\tau} = (10, 110)$, *while the barycenter is* $\boldsymbol{\tau} = (55, 110)$. *The profiles* $\tau_1(t)$ *for both TDAs are depicted in black in Figures 3-(b)(c), and are seen to be discontinuous*[5]. *Now, enlarging slightly* Π *as* $\Pi = \{\boldsymbol{\tau} \,|\, \mathbf{0} < \mathbf{9} \leq \boldsymbol{\tau} \leq \mathbf{111}\}$, *the Slater's condition is satisfied at all time and, as expected, the profiles become continuous as shown in blue in the same graphics. The Analytic Centre can now be computed and the tension profile of the first cable is depicted in Figure 3-(d). One can see that, because of the proximity of the boundary where the tension profile was discontinuous, all TDAs give rise to an abrupt change of the tension.*

---

[3] Or equivalently, the distance to the closest face of Π.

[4] This condition is known as Slater's condition and it is typical in convex optimization. Data not satisfying this condition have no Analytic Centre. This correspond to the very boundary of the WFW, and has no practical impact.

[5] The statement and the proof of the continuity of the Barycenter presented in [21] do not involve Slater's condition, so the example provided here shows it must be not fully correct. The proof of continuity of the norm based TDA given in [35] is difficult, involving continuity of set-valued mappings and Berge maximum theorem. Condition (4.53) in Lemma 4.6 requires that the linear subspace has full dimension within Π, which seems closely related to Slater's condition.

4 THE ANALYTIC CENTRE TENSION DISTRIBUTION ALGORITHM

4.1 Definition and main properties

A cable tension set Ξ, defined as the intersection between Π and the set of convex inequality constraints $\mathcal{C} = \{\boldsymbol{\tau} \,|\, g_i(\boldsymbol{\tau}) \leq 0,\, r = 1, \ldots, r\}$, $\Xi = \Pi \cap \mathcal{C}$ is considered. Then, the (weighted) Analytic Centre is the optimal tension vector $\boldsymbol{\tau}$ that minimizes the function $\phi(\boldsymbol{\tau})$ defined by

$$\phi(\boldsymbol{\tau}) = -\sum_{i=1}^{m} \left(\underline{c}_i \log(\tau_i - \underline{\tau}_i) - \overline{c}_i \log(\overline{\tau}_i - \tau_i) \right) - \sum_{i=1}^{r} \tilde{c}_i \log(-g_i(\boldsymbol{\tau})), \tag{13}$$

subject to the equality constraints $\mathbf{W}\boldsymbol{\tau} + \mathbf{w}_e = \mathbf{0}$. As said previously, the constraints $\boldsymbol{\tau} \in \Pi$ are implicit in this problem formulation and are enforced by the objective logarithmic barriers. From now on, we assume that the equality constraints are feasible with respect to these strict inequality constraints, which corresponds to the Slater's constraint qualification for convex optimization. In practice, this means that the pose is not on the boundary of the WFW.

Remark 4.1. *The requirement of Slater's condition to hold is not a drawback of the Analytic Centre. Most TDAs will fail in computing tensions if the Slater's condition is not satisfied. Moreover, such poses being exactly on the boundary of the WFW have no practical interest.*

The logarithmic barriers are strictly convex constraints in all directions, which, together with the convexity of the logarithmic barriers of the nonlinear constraints, make the function $\phi(\boldsymbol{\tau})$ strictly convex. Therefore, the Analytic Centre is uniquely defined.

The behavior of TDA for time varying poses is of critical importance. Discontinuities in tension profiles or in their derivatives can create unwanted vibrations on the end-effector. Consequently, one asks for tension profiles to be as smooth as possible. Formally, suppose that the pose $\mathbf{p}(t)$ and the external wrench $\mathbf{w}_e(t)$ are k times differentiable. The expression of the wrench matrix $\mathbf{W}(\mathbf{p}(t))$ shows it is as smooth as $\mathbf{p}(t)$. To lighten the notation, in the rest of the paper $\mathbf{W}(t)$ is the same as $\mathbf{W}(\mathbf{p}(t))$. Then, the Analytic Centre $\boldsymbol{\tau}(t)$ is uniquely defined for each time instant by

$$\boldsymbol{\tau}(t) = \underset{\mathbf{W}(t)\boldsymbol{\tau} + \mathbf{w}_e(t) = \mathbf{0}}{\operatorname{argmin}} \phi(\boldsymbol{\tau}). \tag{14}$$

The following Theorem 4.1 shows the smoothness of $\boldsymbol{\tau}(t)$. A proof relying on the application of the implicit function theorem for k times differentiable functions is possible because the optimization problem in Eq.(14) is strictly convex with no inequality constraints[6].

Theorem 4.1. *Let's assume the cost function $\phi(\boldsymbol{\tau})$ strictly convex and, at each instant of time, the optimization problem feasible,[7] while $\mathbf{W}(t)$ is full rank. Provided that $\mathbf{W}(t)$ and $\mathbf{w}_e(t)$ are $k_1 \geq 0$ times differentiable, and that $\phi(\boldsymbol{\tau})$ and $g_i(\boldsymbol{\tau})$ are $k_2 \geq 2$ times differentiable, then the unique solution $\boldsymbol{\tau}(t)$ of the time dependent optimization problem in Eq.(14) is $\min\{k_1, k_2 - 1\}$ times differentiable.*

Proof. Let us consider an arbitrary time instant t_0 and define $\boldsymbol{\tau}_0 = \boldsymbol{\tau}(t_0)$ the unique solution of the optimization problem Eq.(14) for $\mathbf{W}_0 = \mathbf{W}(t_0)$, $\mathbf{w}_{e0} = \mathbf{w}_e(t_0)$. Since the implicit inequality constraints $\underline{\boldsymbol{\tau}} < \boldsymbol{\tau} < \overline{\boldsymbol{\tau}}$ and $g_i(\boldsymbol{\tau}) < 0$ are strict and have, by assumption, some common solutions with the linear

[6] Non strict convexity or change in constraint activation entails non-regularities of the first order conditions Jacobian matrix that prevent applying the implicit function theorem as in the proof of Theorem 4.1.

[7] I.e., the cable tension set defined by $\underline{\boldsymbol{\tau}} < \boldsymbol{\tau} < \overline{\boldsymbol{\tau}}$ and $g_i(\boldsymbol{\tau}) < 0$ intersects the linear subspace $\mathbf{W}(t)\boldsymbol{\tau} + \mathbf{w}_e(t) = \mathbf{0}$.

constraints $\mathbf{W}(t)\boldsymbol{\tau} + \mathbf{w}_e(t) = \mathbf{0}$, they cannot be active and Lagrange theorem can be applied to show that the solution $\boldsymbol{\tau}_0$ of the optimization problem (14) satisfies the system of equations

$$\begin{cases} \nabla\phi(\boldsymbol{\tau}) + \boldsymbol{W}^T\boldsymbol{\mu} = \mathbf{0}, \\ \boldsymbol{W}\boldsymbol{\tau} + \mathbf{w}_e = \mathbf{0}, \end{cases} \tag{15}$$

for $\mathbf{W} = \mathbf{W}_0$ and $\mathbf{w}_e = \mathbf{w}_{e0}$, where $\boldsymbol{\mu}$ is the vector of Lagrange multipliers. This is a square system of equations with variables $\boldsymbol{\tau} \in \mathbb{R}^m$, $\boldsymbol{\mu} \in \mathbb{R}^n$ and where $\mathbf{W}$ and $\mathbf{w}_e$ are regarded as parameters. Every variables and parameters appear linearly in the system of Eq.(15). Note that $\nabla\phi(\boldsymbol{\tau})$ is $k_2 - 1 \geq 1$ times differentiable with respect to $\boldsymbol{\tau}$ (because $\phi(\boldsymbol{\tau})$ is supposed $k_2 \geq 2$ times differentiable). Therefore, the whole system in Eq.(15) is $k_2 - 1$ times differentiable with respect to all variables and parameters. Its Jacobian matrix, with respect to the variables $\boldsymbol{\tau}$ and $\boldsymbol{\mu}$, is

$$\begin{pmatrix} \nabla^2\phi(\boldsymbol{\tau}) & \mathbf{W}^T \\ \mathbf{W} & \mathbf{0}_{n\times n} \end{pmatrix}, \tag{16}$$

which is well known to be regular, provided that $\nabla^2\phi(\boldsymbol{\tau})$ is regular and that $\mathbf{W}$ is full rank. Those conditions are satisfied for $\boldsymbol{\tau}_0$ (because $\nabla^2\phi(\boldsymbol{\tau}_0)$ is symmetric definite positive due to the strict convexity of $\phi(\boldsymbol{\tau})$) and $\mathbf{W}_0$. Therefore, one can apply the implicit function theorem to characterize the variation of the solution $\boldsymbol{\tau}_0$ when parameters $\mathbf{W}_0$ and $\mathbf{w}_{e0}$ change: there exist neighborhoods $\mathcal{N}_{\mathbf{W}}$ of $\mathbf{W}_0$ and $\mathcal{N}_{\mathbf{w}_e}$ of $\mathbf{w}_{e0}$ and solutions $\boldsymbol{\tau}^*(\mathbf{W}, \mathbf{w}_e)$ and $\boldsymbol{\mu}^*(\mathbf{W}, \mathbf{w}_e)$ defined inside those neighborhoods and $k_2 - 1$ times differentiable, which satisfy the system in Eq.(15). Thus, since $\mathbf{W}(t)$ and $\mathbf{w}_e(t)$ are continuous, by definition of the continuity there exists a neighborhood $\mathcal{N}_t$ of t_0 such that, for all $t \in \mathcal{N}_t$, $\mathbf{W}(t) \in \mathcal{N}_{\mathbf{W}}$ and $\mathbf{w}_e(t) \in \mathcal{N}_{\mathbf{w}_e}$. In these neighborhoods, the function $\boldsymbol{\tau}^*(\mathbf{W}, \mathbf{w}_e)$ is $k_2 - 1$ times differentiable, while th functions $\mathbf{W}(t)$ and $\mathbf{w}_e(t)$ are k_1 times differentiable by assumption. Therefore, their composition $\boldsymbol{\tau}^*\big(\mathbf{W}(t), \mathbf{w}_e(t)\big)$ is $\min\{k_1, k_2 - 1\}$ times differentiable. Finally, since the solution to the system of equations at each time instant is unique, $\boldsymbol{\tau}(t) = \boldsymbol{\tau}^*\big(\mathbf{W}(t), \mathbf{w}_e(t)\big)$ inside $\mathcal{N}_t$ and it is $\min\{k_1, k_2 - 1\}$ times differentiable at t_0.

The main peculiarities of the existing TDAs and AC have been given so far. However, the limitations of the AC should still be pointed out to complete the global picture. Therefore, the following Remark aims at highlighting them.

Remark 4.2. *The former drawbacks is related to its iterative nature which, indeed, is typical among all the TDAs based on solving an optimisation problem. The second one is, instead, implicit in the generalised cost function in Eq.*(13). *The possibility to include non-linear constraints can result in upper bound to differentiability given by* $\min\{k_1, k_2 - 1\}$.

4.2 Practical computation of the Analytic Centre

This section aims to show how the use of a suitable solver, to solve the Analytic Centre optimisation problem in Eq.(14), can reduce the computation time of the solution w.r.t. build-in solvers demonstrating real-time capabilities. In particular, the benchmark is made by considering the Sequential Quadratic Program (SQP) algorithm [36] as a representative among the existing ones in the MATLAB library. The choice lies on SQP since it results to be the fastest among the available ones in solving Eq.(14). On the other hand, since the AC has no inequalities to be considered, the Newton's Algorithm 1 is used [34, Sec.10.2]. It is well-known for its quick convergence and sensibility to the choice of the initial iteration. This latter can cause

several problems in terms of convergence. Nonetheless, some stratagems that make the algorithm more robust exist. Indeed, it is possible to adapt the Newton's algorithm to manage infeasible starting points[8] and update the iterant at each solution. Moreover, since the objective function of Analytic Centre is strictly convex, it facilitates the convergence to the solution. All the simulations are performed in MATLAB using a MacBook Pro Retina 2015 with an Intel Core i5 2.7 GHz processor and 8 GB RAM 1867 MHz DDR3. With this aim in mind, let us compare the computational cost of the Newton and MATLAB fmincon-SQP methods to solve the minimization problem in the form of Eq.(14). The scope are to extract and compare the iteration number and computational time of mentioned methods while verifying that the obtained tension profiles coincide. Hereby, the study case considered resolves in a CDPR with 4 cables as depicted in Figure 5-(a): the point-mass is supposed to follow a circular trajectory Eq.(17), of radius $r_c = 0.5\,m$, in 10 seconds where velocity and acceleration are null at the start and end of the path. The mass of the load is set to $20\,kg$ and it is guided by four cables whose tension limits are fixed to $\underline{\tau} = \ 50\,N$ and $\overline{\tau} = 400\,N$, respectively. The trajectory the mass has to follow is described by a circle of equations

$$\begin{cases} x(t) = r_c(\cos(2\pi s(t)) + 1.75) \quad s(t) \in [0,1], \quad t \in [0,10]s, \\ y(t) = r_c(\sin(2\pi s(t)) + 1.75), \end{cases} \tag{17}$$

with $s(t)$ being a 7-degree polynomial with the above-mentioned boundary condition acting up to the 3^{rd} derivative, while the objective function is

$$\phi(\boldsymbol{\tau}) = -\sum_{i=1}^{4} \log(\overline{\boldsymbol{\tau}} - \boldsymbol{\tau}_i) + \log(\boldsymbol{\tau}_i - \underline{\boldsymbol{\tau}}). \tag{18}$$

As far as the computational performance is concerned, the data acquired during the simulation, useful for the comparison, are collected in Table 1. Moreover, in Fig. 4, the computational time necessary to find a solution for each time step simulation is reported. Note that, at each call of the solver, the initial iterant is updated with the previous solution found. Furthermore, observe that the gradient of the cost function $\phi(\boldsymbol{\tau})$ was also provided. Both these expedients are employed to speed up the computation.

Therefore, analysing the data, it seems clear that implementing an ad-hoc algorithm to solve this optimization problem in Eq.(14) helps reducing the computational cost w.r.t. build-in functions. Indeed, Newton is generally 2-order faster than SQP.

Note coherency between the maximum number of iteration and the first call of the Newton method. With SQP, the maximum iteration number does not coincide with the first call. This discrepancies is due to the different architecture of the two algorithms which tackle the problem differently. Briefly, the SQP tries to approximate the objective with a quadratic model and solve the sequence of subproblems. Hence, it generally requires more iterations (and time) to converge. Though the maximum and the initial number of iteration do not coincide for the SQP, the computational time required for the first iteration results coherent, for both algorithms, as the most expensive, due to the distance between the initial (i.e. tentative) and the first solution.

To conclude, it is worth noticing the Newton trend in Fig. 4: it is evident the presence of two steps at the start and end of the simulation. These are due to non-homogeneous distribution of the points along the trajectory which, because of $s(t)$, are more dense about the start and end of the path. The quick convergence of the method makes it sensible to the discretization of the trajectory.

[8]This means that the initial iterant satisfies the tension limits but does not necessarily satisfy the equilibrium Eq.(1).

Table 1: Summary of the simulation data

Results	Newton	fmincon-SQP
Time Step	$0.001s$	$0.001s$
n_{iter} First Solution	5	10
Mean Computational Time	$6.7e^{-5}\frac{s}{sol.}$	$6.7e^{-3}\frac{s}{sol.}$
Max. Iteration Number	5	42
Stopping Criterion	$\|\|Eq.(15)\|\| < 10^{-10}$	function and step tolerances

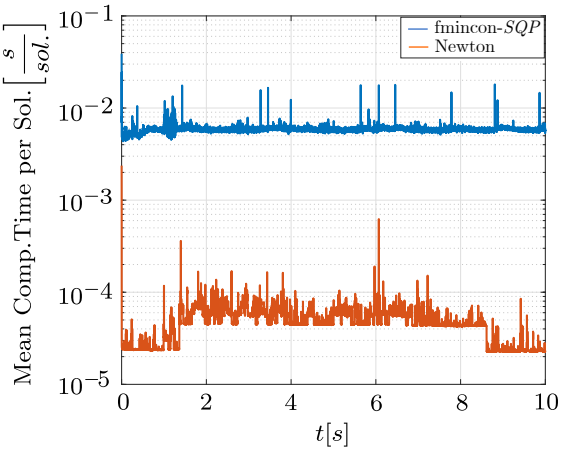

Fig. 4: Step time comparisons between Newton and fmincon-SQP algorithms. This graph represents the mean value of computational times. It is averaged over three simulations in order to reduce the passive effects of other processes running in parallel on the processor.

Moreover, looking at both trends, it seems that Newton oscillates more than SQP. This is due to passive processes ongoing on the laptop. Indeed, their influence affect more the Newton trend since it works 2-order faster than SQP: a disturbance has minor effect over a big quantity.

Algorithm 1 Newton Algorithm [see [34], pag. 531]

Input: $\boldsymbol{\tau}_0$ % generally $\hat{\boldsymbol{\tau}}$
While: $||Eq.(15)|| >$ Tol & iter $<$ Max$_{\text{iter}}$
Compute: $\boldsymbol{\tau}_{k+1}$
Update: $\boldsymbol{\tau}_0 \rightarrow \boldsymbol{\tau}_{k+1}$
End
Output: $\boldsymbol{\tau}$ % last $\boldsymbol{\tau}_0$

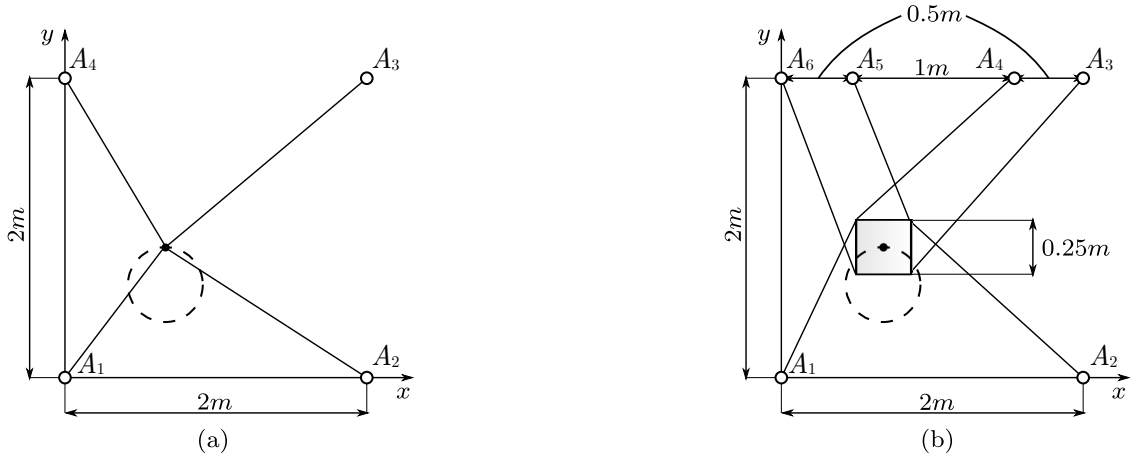

Fig. 5: Two planar CDPRs: (a) composed of four cables and a point-mass end-effector, (b) composed of six cables and a rigid-body platform end-effector

5 SIMULATIONS AND CASE STUDIES

The implementation of the Analytic Centre, defined in Sec. 4-C, to different case studies is conveyed in this section. In accordance with the previous tension distribution methods, mostly developed for CDPRs, this section will follow the same explanatory line to emphasize the peculiarities of the Analytic Centre, even though it applies for a wide range of CDPs [3, 37]. In particular, planar CDPRs with four and six cables and a planar MCDPR with four cables will be considered. In addition, also a spatial CDPR with eight cables is studied. Their dynamics will be simulated while cable tension profiles are computed using the Analytic Centre and various state-of-the-art methods. Indeed, the purpose of this section is to show and compare the capabilities of the Analytic Centre with respect to previous works in order to get its pros and cons. With this in mind, a total of four examples will be considered to reveal its main peculiarities.

In the first case study, Sec.5.1, the comparison with existing methods will focus on robustness, continuity and differentiability of the solutions.

The second example, Sec.5.2, aims to highlight the *generality* of the proposed method, illustrating the possibility to apply it with any DoR while providing feasible, robust and smooth tension profile solutions. Furthermore, the computational time of the methods that are capable of providing a feasible and continuous solution with general DoR is compared to confirm that the proposed method can operate in real-time.

The third case study described in Sec.5.3 lends itself well to emphasize the *versatility* of the Analytic Centre. Indeed, it shows that it is possible to take into account non-linear time-varying constraints in a natural way, returning, again, a set of tensions with the aforementioned characteristics. Observe that non-linear constraints can be considered only with the AC method.

To conclude, the last simulation, Sec.5.4, somehow summarizes all the previous results, demonstrating the Analytic Centre capabilities even when a spatial case is considered.

5.1 Planar CDPR composed of four cables and a point-mass end-effector

The architecture of the robot considered in this study, as well as the trajectory, is the same used in Section 4.2.

During the tracking task, the robust index defined in Eq.(10) is computed. Moreover, several state-of-the-art methods are reproduced to determine the tension profiles according to different criteria. The obtained results are collected and depicted in Figure 6. At a first sight, all implemented methods provide

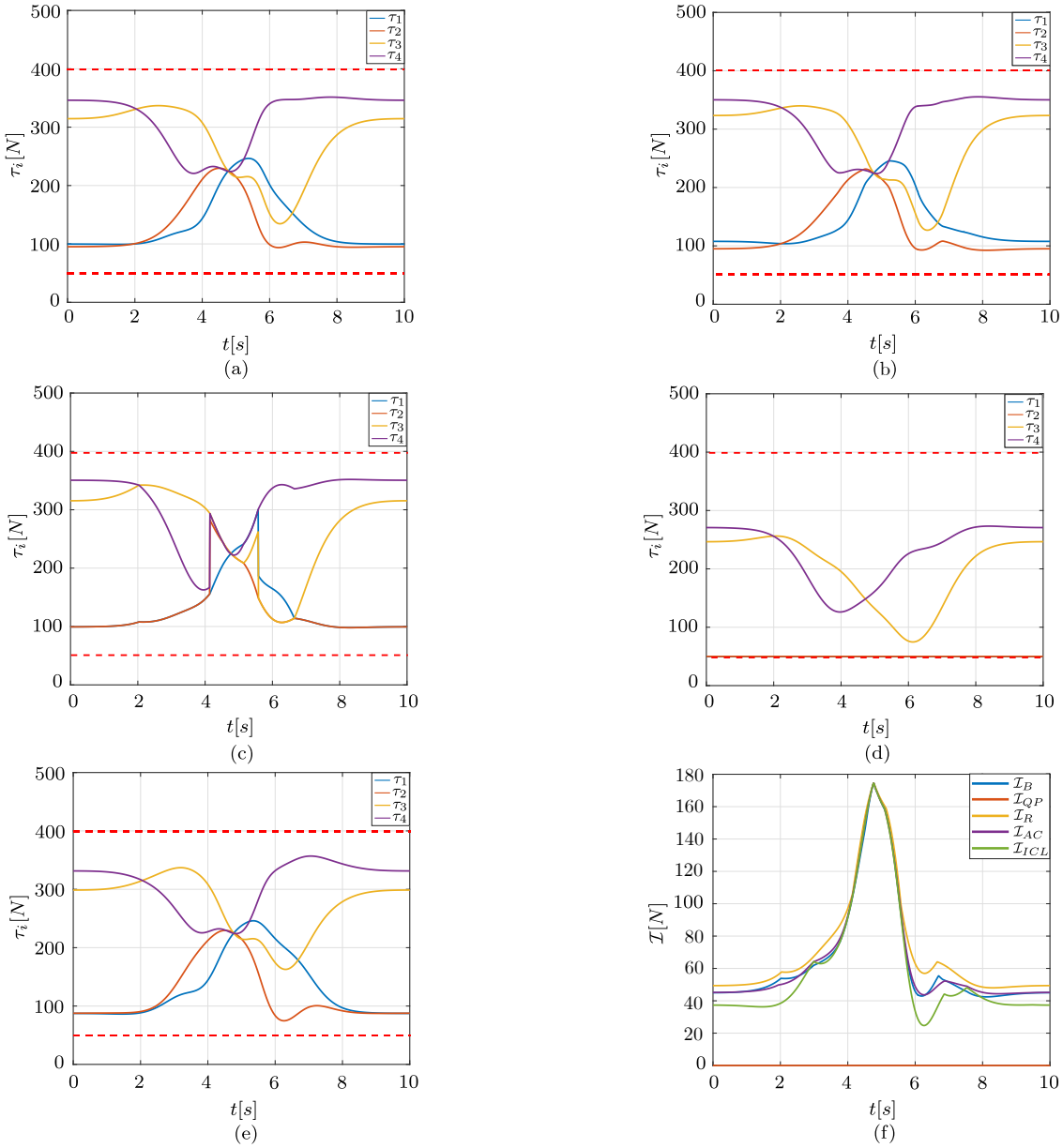

Fig. 6: Tension profiles for: (a) Analytic Centre approach, (b) Barycentric method, (c) Robust (LP) technique, (d) Quadratic Programming (QP) and (e) Improved-Closed Form. The trends of the robust index for the mentioned methods are reported in Figure (f).

feasible solutions: the tension profiles found satisfy the maximum and minimum tension constraints of Eq.(4) (represented in each figure by the dashed red line) and the load equilibrium in Eq.(1). Moreover, the profiles look not symmetric since the trajectory has been shifted in the left-bottom corner of the robot workspace. The considered methods are now investigated one-by-one in order to remark on the relevant aspects necessary for the comparison.

Let's consider the QP method first, whose tension profiles are depicted in Fig.6-(d) [17]. This approach tends to save energy required from the actuators by minimizing the tension components as much as possible.

Indeed, the results show that two tension components τ_1 and τ_2 (cables below the load) are found to assume the minimum value. As a result, the robustness index is the lowest among the other methods, as shown in Fig.6-(f). In practice, tension profiles are continuous and differentiable but the robot suffers from low stiffness which can lead to undesired vibrations and oscillations of the platform.

On the other hand, the Robust solution reported in Fig.6-(c) is the one that has the highest robustness index value. However, since this approach belongs to the family of LP optimization methods [12], the solution can result in discontinuities. This example reveals discontinuities of the solution while tracking a smooth circular trajectory. In some sense, achieving the maximum stiffness is akin admitting discontinuities in the tension profiles. Therefore, the presence of discontinuities, even when continuous trajectory and wrench are considered, can cause unwanted phenomena (e.g. vibrations) on the end-effector.

In Figure 6-(b), the solution found using the Barycentric approach [27, 21] is similar in both tension profiles and the robustness is similar to the Analytic Centre solution reported in Fig. 6-(a). Despite their affinity, there are crucial differences among them. Indeed, although the Barycentric provides robust and continuous profiles, there is no formal evidence of their differentiability. Moreover, even though this technique is general and then valid for any DoR, the sudden increase of computational cost makes it unfeasible already for $DoR = 3$. This latter will be better clarified in the next section.

The Improved-Closed Form [22] approach, whose solution is displayed in Fig.6-(e), gives continuous tension profiles with a close, but generally lower, robustness index value than the Analytic Centre method. It constitutes an improvement to the previous work [23]. Anyway, the absence of a formal proof, guaranteeing the convergence to a feasible solution, represents the main shortcoming of this approach.

So far, for the considered methods in the literature, the robustness, continuity and differentiability of the tensions were discussed. To sum up, these examples showed that, among these TDAs, the Analytic Centre is the only one able to preserve the mentioned properties simultaneously.

5.2 Planar CDPR composed of six cables and a rigid-body platform end-effector

The use of several cables serves as an example to demonstrate the generality w.r.t. DoR of the proposed method in finding a robust solution which is also continuous and differentiable. The scheme of the robot is depicted in figure 5-(b). The centre of mass of the square platform is supposed to follow the same trajectory as in the previous case of Sec.5.1. The axes of the mobile reference frame will remain parallel to those of the fixed one throughout the simulation. The mass of the load is $65\,kg$ and it is guided by six cables whose tension limits are the same as in the previous example. The choice of a large mass forces the system to the boundary of the WFW.

Simulation results are given in Figure 7. Observe that, because of the several cables, $DoR = 3$ and therefore the Barycentric approach can not be applied. Indeed, the existing method [27, 21] relies on finding the barycenter of a 2D polytope Λ, defined in Eq.(7), by means of triangulation techniques. The latter can be efficiently applied in a low-dimensional space. Already from a dimension higher than two, this technique results impractical due to the increase in its computational cost. This issue, combined with the common structure of CDPRs, which often foresees a maximum of $DoR = 2$, prevented from a generalization. Anyway, the advent of CDP where a large redundancy can occur is, among the others, another motivation for the introduction of the Analytic Centre.

The Improved Closed-Form method, instead, fails in furnishing a feasible solution. This happens because the high mass pushes the cable tensions outside the limits. Hence, although it is an improved version of the Closed-Form method [23], it is not always able to converge in DoR steps. The same authors express this possibility in their work [22]. Thus, this case study identifies a reduced WFW coverage of the Improved Closed-Form w.r.t. the Analytic Centre, QP and Robust methods which find a feasible solution.

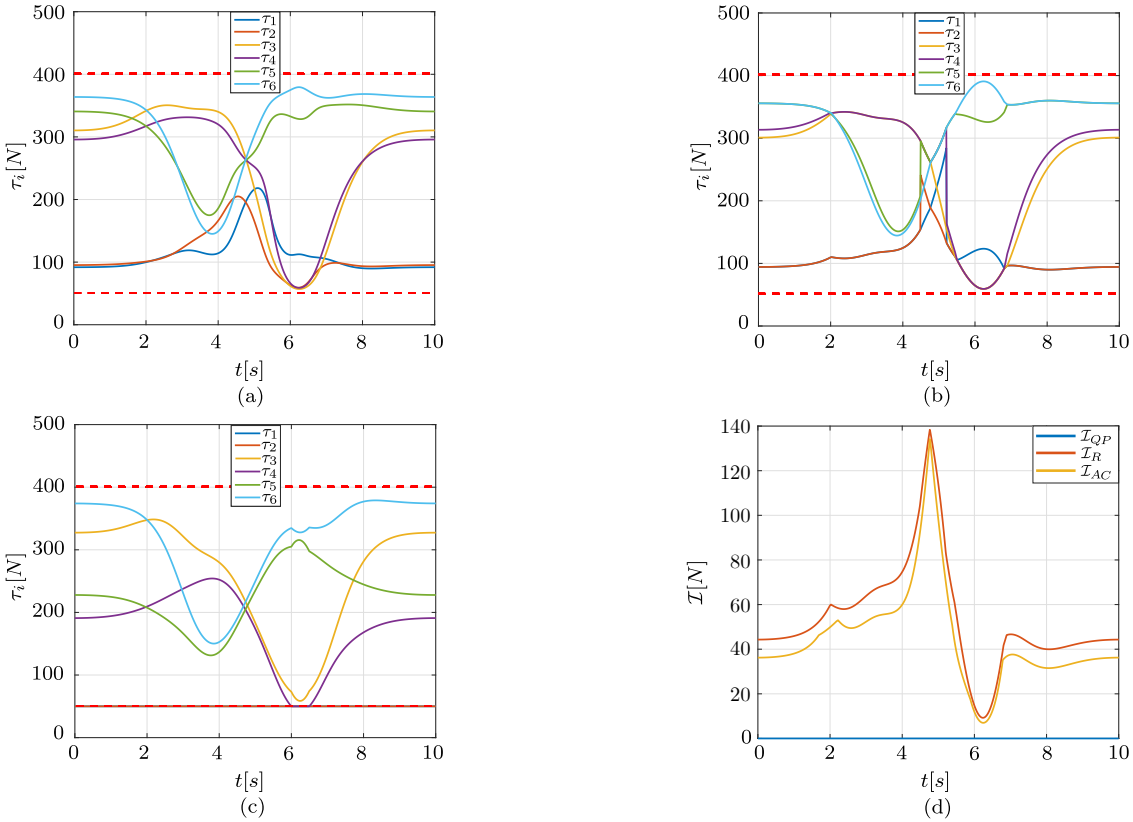

Fig. 7: Tension profiles for: (a) Analytic Centre, (b) Robust (LP) method and (c) Quadratic Programming (QP). The trends of the robustness index for the mentioned methods are reported in Figure (d).

Among the remaining methods, whose solutions are reported in Fig.7, the Analytic Centre approach appears to be the best compromise between robustness and continuity of the solution. Indeed, looking at Figure 7-(d), the QP maintains the lowest robustness index, reducing the energy consumption at the price of a reduced stiffness of the robot, whereas the Robust method registers the highest index value but introduces discontinuities of tensions in time which can cause unwanted phenomena as well.

However, at this point, someone might wonder what is the performance of this method in terms of computational time. Hence, to make a fair comparison, the computational time required to determine the solution for each optimization problem is considered. In this regard, a comparison of the approaches that return *regular* continuous and feasible tension profiles for any DoR is given.

The graph in Fig.8 shows the time required by the solver to find a solution during the simulation for both the Analytic Centre and QP methods. In particular, these data are generated by averaging the solution times over 3 simulations to remove disturbances that can occur due to passive processes ongoing on the computer. For the Analytic Centre approach, the Newton algorithm discussed in 4.2 is used to solve the optimization problem whereas, for the QP method, the Sequential Quadratic Programming (SQP) algorithm [36] is a natural choice, given the nature of the problem. The gradient of the objective function are provided in advance as well as the iterant are updated at each call, in order to speed up the solvers.

Looking at the graph in Fig.8, the computational times of the Newton method applied to the Analytic Centre is 2-order smaller than the QP. The differences in the iteration time are to be attributed to the diversity between the solvers, the objective functions and the absence of active constraints (i.e. inequalities) in the

Table 2: Summary of the simulation data

Results	Newton (AC)	fmincon-SQP (QP)
Time Step	$0.001s$	$0.001s$
n_{iter} first Solution	7	2
Mean Computational Time	$7.3e^{-5}\frac{s}{sol.}$	$6.8e^{-3}\frac{s}{sol.}$
Max. Iteration Number	7	3
Stopping Criterion	$\|\|Eq.(15)\|\|_2 < 10^{-10}$	function and step tolerances

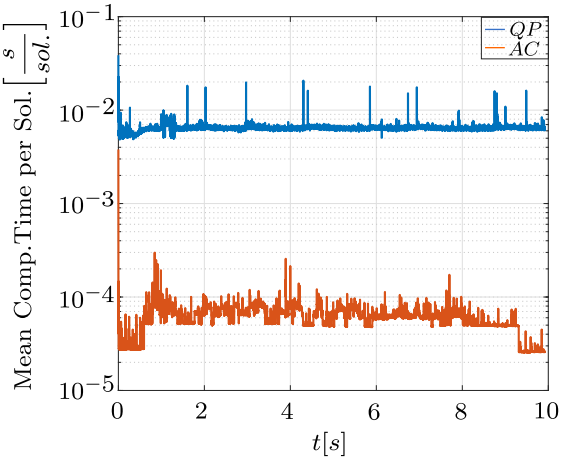

Fig. 8: Computational time per solution during the simulation. This graph represents the mean value of the computational times. It is averaged over three simulations in order to reduce the passive effects of other processes running in parallel on the processor.

case of the Analytic Centre approach. The inequalities which define the QP optimization problem increase its complexity, forcing the solver consuming time for the few iterations required to converge. In both cases, the first iteration is the one which costs more. The maximum number of iterations recorded amounts to $n_{iter,AC} = 7$ and $n_{iter,QP} = 3$. Because the QP method is generally applied in real-time applications, it is reasonable to argue that also the Analytic Centre can be applied in real-time to control the cable tensions of a CDP. Table 2 summarizes the discussed data used for time comparisons.

5.3 Planar MCDPR composed of four cables and a point-mass end-effector

This example takes its cue from mobile cable systems [30, 29]. Indeed, in these systems, the choice of the cable tensions has to take into account the static friction between the ground and the Mobile Base (MB) to avoid sliding effects during the execution of a task. This motivates the need to introduce non-linear constraints in the cable tensions computation. The scheme of the MCDPR considered in this example is given in Fig. 9. It constitutes a simplified version of the original MCDPRs. Indeed, in practice, friction is considered to act on the four wheels that move each MB instead of assuming its influence as concentrated on its centre of mass. However, this architecture is enough for the scope of this section and, although it

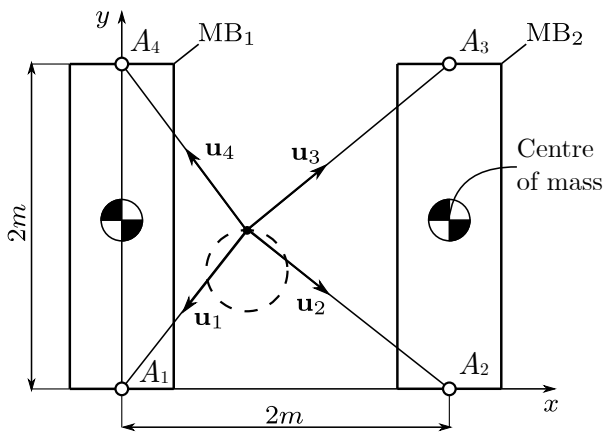

Fig. 9: Architecture of a planar MCDPR with 4 cables

constitutes a simplified model, it does not represent a limitation for the presented method. Later on, the MBs will be considered as fixed at the ground and therefore the robot will coincide with the study case discussed in Sec. 5.1. This latter will allow to make comparisons and see the consequences on the MCDPR due to the differences in the tensions distribution when friction is not considered.

For the current case, the mass of the moving base is considered to be equal to $m_{\text{MB}_1} = m_{\text{MB}_2} = 65kg$ while the load mass is $5kg$. The static friction coefficient is $\mu = 0.5$. The load trajectory is the same as in the previous cases, and the same are the tension limits.
The equations which constitute the non-linear constraints $\mathcal{C}$ for the cable tensions are the followings

$$||\tau_1\mathbf{u}_1 + \tau_4\mathbf{u}_4||_2^2 \leq m_{\text{MB}_1}^2\, g^2\, \mu^2, \quad ||\tau_2\mathbf{u}_2 + \tau_3\mathbf{u}_3||_2^2 \leq m_{\text{MB}_2}^2\, g^2\, \mu^2. \tag{19}$$

These can be derived by using the free-body diagram for both MB_1 and MB_2. Indeed, the MB can be considered as decoupled systems.
The computed tension profiles are depicted in Fig.10a. The objective function used for this simulation is reported in Eq. (20) for sake of clarity.

$$\begin{aligned}\boldsymbol{\phi}(\boldsymbol{\tau}) = -\Big(\sum_{i=1}^{4}\log(\tau_i - \tau_{min,i}) + \sum_{i=1}^{4}\log(\tau_{max,i} - \tau_i) + \log\big(-\big(\tau_1+\tau_4\big)^2 + m_{\text{MB}_1}^2\, g^2\, \mu^2\big) \\ + \log\big(-\big(\tau_2+\tau_3\big)^2 + m_{\text{MB}_2}^2\, g^2\, \mu^2\big)\Big).\end{aligned} \tag{20}$$

The tension profiles show how the introduction of friction narrows the set of tensions that can be used to perform a task. In particular, the tensions, Fig.10a continuous line, assume reduced values compared to the case of fixed moving bases. In other words, avoiding sliding conditions for the MBs means reducing the tension values while performing a task. The consequences of neglecting friction while computing tension profiles can be visualized in Fig.10b. The trend of the constraints demonstrates that neglecting friction can cause the MBs to slide since the dotted curves exceed the static friction limit. An alternative way to display the same phenomena consists in investigating if the $\boldsymbol{\lambda}$ vectors of the two solutions, for $t = 3s$ and $t = 5s$, belong to the intersection between the feasible polygon and the non-linear constraints $\hat{\Xi} = \Lambda \cap \mathcal{C}$; the dual of Ξ. The equations necessary to map the constraints into Λ, as done in Figs.11a and 11b, are the followings

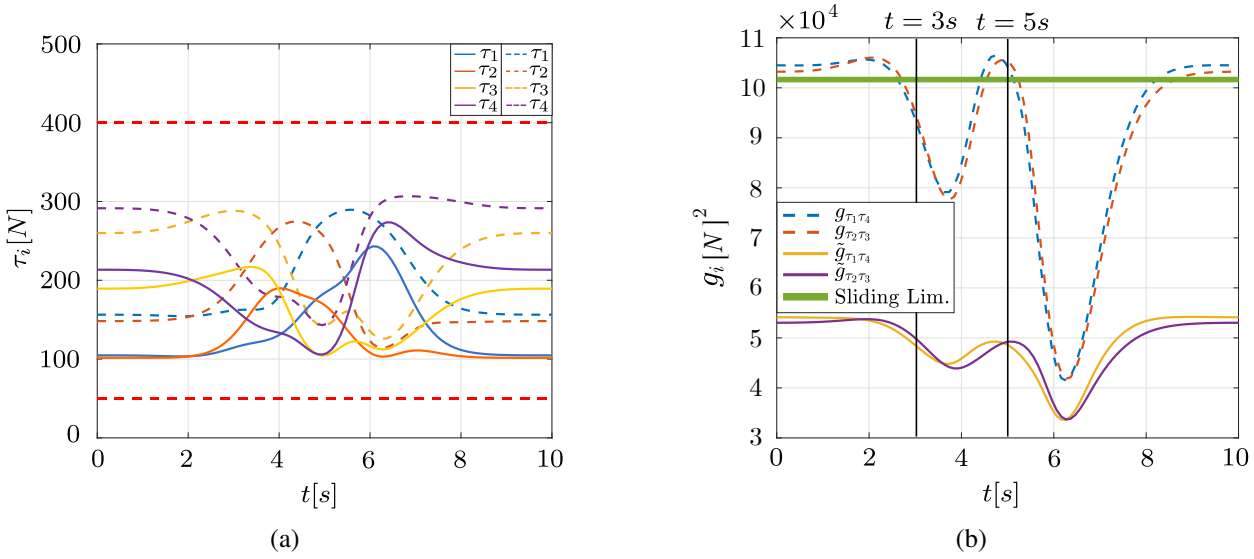

(a) (b)

Fig. 10: Comparisons of the results: Fig.(a) reports the cable tension for the MCDPR. The solid-line profiles refer to the case with non-linear constraints, whereas the dotted ones do not consider any additional constraints (i.e. the MBs are considered as fixed). Fig.(b) shows the trend of the non-linear constraint values of Eq.(19) for the two MBs. The constraints $\tilde{g}_{\tau_1\tau_4}$ and $\tilde{g}_{\tau_2\tau_3}$ take friction into account, while $g_{\tau_1\tau_4}$ and $g_{\tau_2\tau_3}$ do not. It can be seen that, for the present case, the $g_{\tau_i\tau_j}$ (dotted profiles) constraints exceed the sliding limit several times.

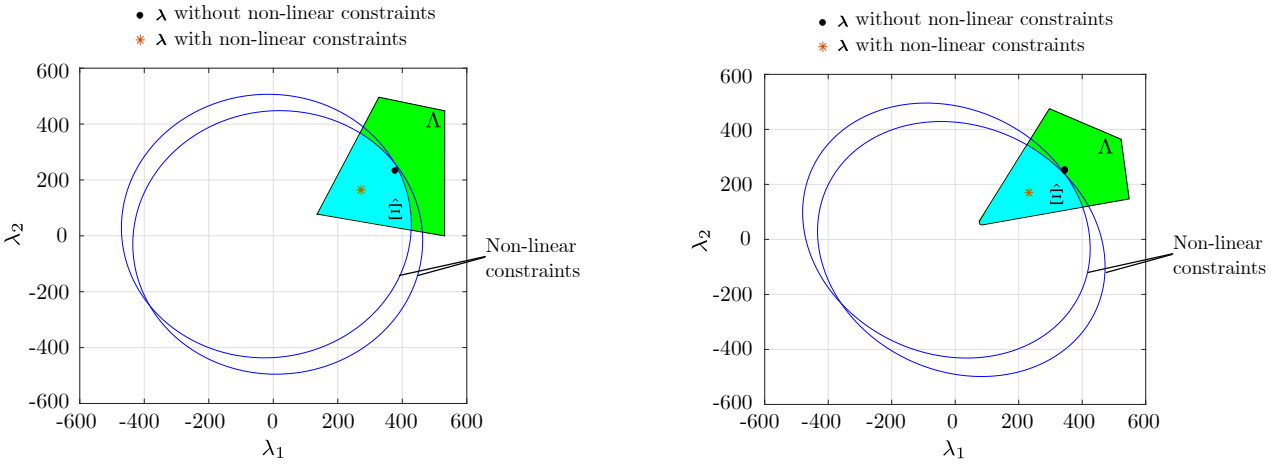

(a) (b)

Fig. 11: Intersection between the feasible polygon Λ and the non-linear constraints in Eq.19. These plots depict the case at (a) $t = 3s$ and (b) $t = 5s$. Notice that only the $\boldsymbol{\lambda}$ vector computed by considering the non-linear constraints is feasible in both cases.

$$\boldsymbol{\tau}_{p,1}^2 + (\mathbf{N}\boldsymbol{\lambda})_1^2 + 2\boldsymbol{\tau}_{p,1}(\mathbf{N}\boldsymbol{\lambda})_1 + \boldsymbol{\tau}_{p,4}^2 + (\mathbf{N}\boldsymbol{\lambda})_4^2 + 2\boldsymbol{\tau}_{p,4}(\mathbf{N}\boldsymbol{\lambda})_4 + 2\big(\boldsymbol{\tau}_{p,1}\boldsymbol{\tau}p,4 + \boldsymbol{\tau}_{1,p}(\mathbf{N}\boldsymbol{\lambda})_4 + \boldsymbol{\tau}_{4,p}(\mathbf{N}\boldsymbol{\lambda})_1 + (\mathbf{N}\boldsymbol{\lambda})_1(\mathbf{N}\boldsymbol{\lambda})_4\big) \leq m_{\text{MB}_1}^2\, g^2\, \mu^2, \tag{21a}$$

$$\boldsymbol{\tau}_{p,2}^2 + (\mathbf{N}\boldsymbol{\lambda})_2^2 + 2\boldsymbol{\tau}_{p,2}(\mathbf{N}\boldsymbol{\lambda})_2 + \boldsymbol{\tau}_{p,3}^2 + (\mathbf{N}\boldsymbol{\lambda})_3^2 + 2\boldsymbol{\tau}_{p,3}(\mathbf{N}\boldsymbol{\lambda})_3 + 2\big(\boldsymbol{\tau}_{p,2}\boldsymbol{\tau}p,3 + \boldsymbol{\tau}_{2,p}(\mathbf{N}\boldsymbol{\lambda})_3 + \boldsymbol{\tau}_{3,p}(\mathbf{N}\boldsymbol{\lambda})_2 + (\mathbf{N}\boldsymbol{\lambda})_2(\mathbf{N}\boldsymbol{\lambda})_3\big) \leq m_{\text{MB}_1}^2\, g^2\, \mu^2, \tag{21b}$$

where $\boldsymbol{\tau}_{p,i}$ and $(\mathbf{N}\boldsymbol{\lambda})_i$ represent the components of the particular and general solution presented in Eq.(6), respectively. Thus, the constraint Equation (21) describes the ellipses in Figs. 11a-11b and they can be retrieved by substituting Eq.(6) into Eqs.(19). In other words, it suffices to employ the composition rule for functions. Furthermore, observe that the elements $(\mathbf{N}\boldsymbol{\lambda})_i$ could be thought as $\boldsymbol{\tau}_{g,i}$ but, here, the explicit version with $\boldsymbol{\lambda}_i$ is clearer since the aim is to investigate the conic constraint intersection with the feasible polygon Λ. Indeed, as a confirmation of what displayed in Fig.10b, Figs.11a and 11b demonstrate that the sliding condition occurs when $\boldsymbol{\lambda} \notin \hat{\Xi}$.

This example showed the ability of the Analytic Centre to deal with non-linear constraints, so far approximated as linear, as in [30, 29], for example. In addition, as done in Eq.(20), the possibility to *superimpose* general (linear and non-linear) time-varying constraints on specific cable tensions makes this approach compatible with Human Physical-Interaction (HP-I) or collaborative applications. Indeed, the mentioned applications ask to cope with humans, thus demanding to take precautions in terms of tension limit along specific cables which, usually, are close to a human [38].

5.4 Spatial CDPR composed of eight cables and a rigid-body end-effector

This example is intended to summarise the distinctive features of the TDAs analysed and the one proposed here. In particular, a spatial CDPR designed for collaborative tasks will be considered [38]. This robot considers eight cables and has 2 $DoRs$. The cables are fixed at the upper part of the frame, near the vertices of the cubic cell, as shown in the Figure 12[9]. This choice avoids possible dangerous contact with the operator intent on collaborating with the platform.

For the purposes of the paper, it is sufficient to consider a tracking task: the trajectory under consideration is always circular and arranged in the horizontal plane of Eq.(22), similar to the previous cases. The full dimension of the robot and its precise description can be found in [38]. The mass of the platform is $m = 7kg$ and it is guided by eight cables whose tension limits are fixed to $\underline{\tau} = 1\,N$ and $\overline{\tau} = 100\,N$, respectively. The trajectory the mass has to follow is a circle centered in the robot frame at 2m high from the ground

$$\begin{cases} x(t) = r_c \cos(2\pi s(t)) \quad s(t) \in [0,1], \quad t \in [0,10]s, \\ y(t) = r_c \sin(2\pi s(t)), \\ z(t) = 2. \end{cases} \tag{22}$$

As done for the other case study, several TDAs are compared. Their tension profiles and robustness indices are reported in Fig.13. Alike the case study in Section 5-A, all the methods provide feasible tension

[9]The real prototype is located in Nantes, France at LS2N.

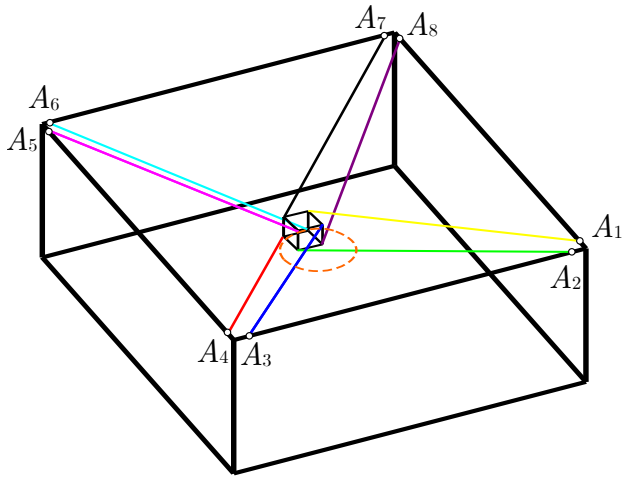

Fig. 12: Spatial architecture considered, see [38] for details.

profiles and pertain to the main characteristics discussed above. However, as seen before, the existing methods result in optimal performances only for particular, predefined, operating conditions. In fact, in many cases (for certain tasks), some of their relevant properties are lost, such as continuity of tension profile, quick convergence, generality for any DoR, and so on.

A further aspect to be examined and added to the previous considerations is highlighted by the architecture considered. Indeed, this CDPR is redundant but not fully-constrained as the load is suspended. In the several case studies analysed in the state of the art, this type of architecture is not very common but nevertheless it is important for some recent applications.

In particular, the major difference that is evident, compared to the previous examples, concerns the values taken by the robustness indices.

In fact, this time, the QP method, see Fig.13-(d), does not have the lowest index. Moreover, the other methods show relatively little difference in terms of robustness. In some ways, they can be considered equivalent.

In case of a suspended loads, it has been seen [39] that the capability to optimise the cable tension is reduced. In other words, the absence of cables under the platform leads to a reduction of the area (hyper volume, in general) of the polygon Λ and thus in a reduced ability to generate a wrench on the load. This, also, explains why the range of variation of the various robustness indices is small compared to the previous cases (all fully-constrained). All indices are very similar to each other with the robust method, as always, holding the maximum value.

To conclude, this example confirms that, in general, the existing methods result in optimal performances only for particular predefined operating conditions (i.e. task at hand and architecture). Instead, the Analytical Centre method always guarantee the best compromise in terms of robustness, smoothness of tension profiles, generality, and reliability.

6 CONCLUSIONS

In this paper, the tension distribution problem for Cable-Driven Platforms (CDPs) with $DoR \geq 1$ was addressed. The formulation of the optimization problem with the barrier function enabled eliminating inequality constraints, considering non-linear constraints and reaching a robust and unique solution in the tension space. Therefore, this made unnecessary to develop additional algorithms for building Λ polytopes

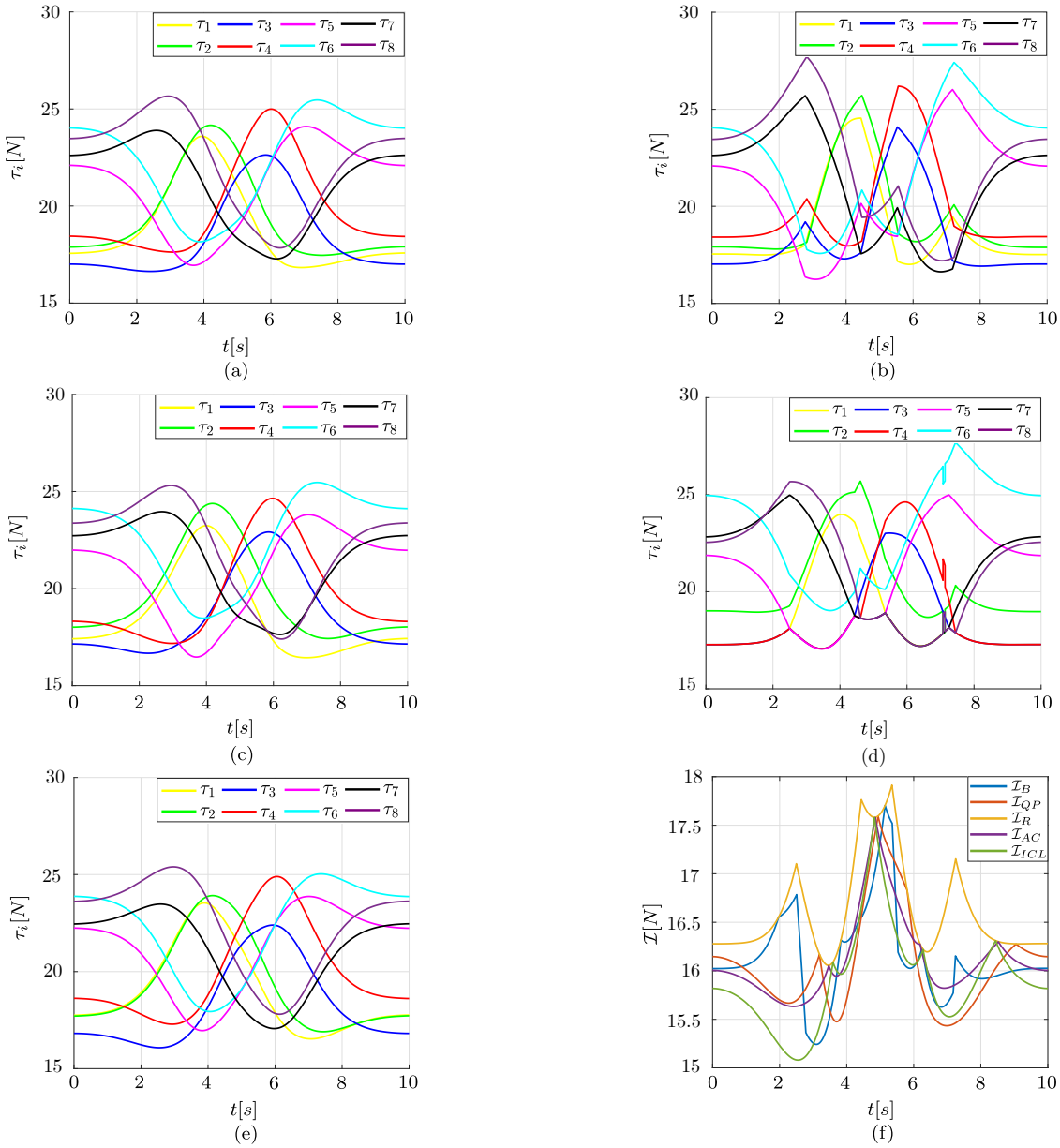

Fig. 13: Tension profiles for: (a) Analytic Centre approach, (b) Barycentric method, (c) Quadratic Programming (QP), (d) Robust (LP) technique and (e) Improved-Closed Form. The trends of the robustness index for the mentioned methods are reported in (f). Observe that the colors used for the tension profiles coincide with the colors of the cables in Fig. 12.

that are complex for high Degree of Redundancy (DoR). Moreover, using the Analytic Centre, cable tension profiles were proven to be continuous and differentiable. The proposed examples showed that the Analytic Centre is the best compromise among the reproduced methods in terms of robustness, continuity and differentiability. The computational aspect was also considered, in fact, the implementation of the Newton method allowed to demonstrate its real-time capabilities. Finally, this method is not only general, but its versatility extends its applicability to a wide range of cable robots such as MCDPRs and ACTSs. Therefore, it lays the

first brick towards tension management for collaborative tasks. Future work deals with the implementation of this technique on a real framework.

REFERENCES

[1] Pott, A., 2018, "Cable-driven parallel robots," *Springer Tracts in Advanced Robotics*.

[2] Villa, D., Brandão, A., and Sarcinelli-Filho, M., 2020, "A survey on load transportation using multirotor uavs," *Journal of Intelligent and Robotic Systems: Theory and Applications*.

[3] Jamshidifar, H., and Khajepour, A., 2020, "Static workspace optimization of aerial cable towed robots with land-fixed winches," *IEEE Transactions on Robotics*.

[4] Albus, J., Bostelman, R., and Dagalakis, N., 1993, "The nist robocrane," *Journal of Robotics System*.

[5] Merlet, J., and Daney, D., 2010, "A portable, modular parallel wire crane for rescue operations," *IEEE International Conference on Robotics and Automation*.

[6] G. Rosati, P. G., and Masiero, S., 2007, "Design, implementation and clinical tests of a wire-based robot for neurorehabilitation," *IEEE Transactions on Neural Systems and Rehabilitation Engineering*.

[7] D. Surdilovic, J. Z., and Bernhardt, R., 2007, "String-man: Wire-robot technology for safe, flexible and human-friendly gait rehabilitation," *IEEE 10th International Conference on Rehabilitation Robotics*.

[8] Cone, L. L., 1985, "Skycam: An aerial robotic camera system," *BYTE*.

[9] Michael, N., Fink, J., and Kumar, V., 2010, "Cooperative manipulation and transportation with aerial robots," *Robotics: Science and Systems*.

[10] Di Paola, V., Goldsztejn, A., Zoppi, M., and Caro, S., 2023, "Design of a sliding mode-adaptive pid control for aerial systems with a suspended load exposed to wind gusts," *Journal of Computational and Nonlinear Dynamics*.

[11] Bosscher, P., Williams, Robert L., I., and Tummino, M., 2005, "A concept for rapidly-deployable cable robot search and rescue systems," *International Design Engineering Technical Conferences and Computers and Information in Engineering Conference*.

[12] Borgstrom, P. H., Jordan, B. L., Sukhatme, G. S., Batalin, M. A., and Kaiser, W. J., 2009, "Rapid computation of optimally safe tension distributions for parallel cable-driven robots," *IEEE Transactions on Robotics*.

[13] Wei-Jung Shiang, D. C., and Gorman, J., 2000, "Optimal force distribution applied to a robotic crane with flexible cables," *IEEE International Conference on Robotics and Automation*.

[14] Oh, S.-R., and Agrawal, S. K., 2003, "Cable-suspended planar parallel robots with redundant cables: controllers with positive cable tensions," *IEEE International Conference on Robotics and Automation*.

[15] Gosselin, C., and Grenier, M., 2011, "On the determination of the force distribution in overconstrained cable-driven parallel mechanisms," *Meccanica*.

[16] Verhoeven, R., and Hiller, M., 2002, "Tension distribution in tendon-based stewart platforms," *Lenarčič, J., Thomas, F. (eds) Advances in Robot Kinematics*.

[17] Taghirad, H. D., and Bedoustani, Y. B., 2011, "An analytic-iterative redundancy resolution scheme for cable-driven redundant parallel manipulators," *IEEE Transactions on Robotics*.

[18] Agahi, M., and Notash, L., 2009, "Redundancy resolution of wire-actuated parallel manipulators," *Transactions of the Canadian Society for Mechanical Engineering*.

[19] Hassan, M., and Khajepour, A., 2008, "Optimization of actuator forces in cable-based parallel manipulators using convex analysis," *IEEE Transactions on Robotics*.

[20] Hassan, M., and Khajepour, A., 2011, "Analysis of bounded cable tensions in cable-actuated parallel manipulators," *IEEE Transactions on Robotics*.

[21] Mikelsons, L., Bruckmann, T., Hiller, M., and Schramm, D., 2008, "A real-time capable force calcula-

tion algorithm for redundant tendon-based parallel manipulators," *2008 IEEE International Conference on Robotics and Automation*.

[22] Pott, A., 2013, "An improved force distribution algorithm for over-constrained cable-driven parallel robots," *6th International Workshop on Computational Kinematics (CK)*.

[23] Pott, A., Bruckmann, T., and Mikelsons, L., 2009, "Closed-form force distribution for parallel wire robots," *Kecskeméthy, A., Müller, A. Computational Kinematics. Springer, Berlin, Heidelberg*.

[24] Bouchard, S., Gosselin, C., and Moore, B., 2010, "On the ability of a cable-driven robot to generate a prescribed set of wrenches," *Journal of Mechanisms and Robotics*.

[25] Katharina Müller, C. R., and Bruckmann, T., 2014, "Analysis of a real-time capable cable force computation method," *Cable-driven Parallel Robots: Proceedings of the Second International Conference on Cable-Driven Parallel Robots, Springer International Publishing*.

[26] Côté, A. F., Cardou, P., and Gosselin, C., 2016, "A tension distribution algorithm for cable-driven parallel robots operating beyond their wrench-feasible workspace," *16th International Conference on Control, Automation and Systems (ICCAS)*.

[27] Gouttefarde, M., Lamaury, J., Reichert, C., and Bruckmann, T., 2015, "A versatile tension distribution algorithm for n-dof parallel robots driven by $n + 2$ cables," *IEEE Transactions on Robotics*.

[28] Ueland, E., Sauder, T., and Skjetne, R., 2020, "Optimal force allocation for overconstrained cable-driven parallel robots: Continuously differentiable solutions with assessment of computational efficiency," *IEEE Transactions on Robotics*.

[29] Tahir Rasheed, Philip Long, D. M.-G., and Caro, S., 2018, "Tension distribution algorithm for planar mobile cable-driven parallel robots," *Cable-Driven Parallel Robots. Mechanisms and Machine Science. Springer,Cham*.

[30] Rasheed, T., Long, P., and Caro, S., 2020, "Wrench-feasible workspace of mobile cable-driven parallel robots," *Journal of Mechanisms and Robotics*.

[31] Xiong, H., Cao, H., Zeng, W., Huang, J., Diao, X., Lu, W., and Lou, Y., 2022, "Real-time reconfiguration planning for the dynamic control of reconfigurable cable-driven parallel robots," *J. Mech. Robot.*

[32] Tobias Bruckmann, A. P., and Hiller, M., 2006, "Calculating force distributions for redundantlyactuated tendon-based stewart platforms," *Advances in Robot Kinematics (ARK), Ljubljana, Slovenia. Springer-Verlag*.

[33] Nesterov, Y., and Nemirovskii, A., 1994, *Interior-Point Polynomial Algorithms in Convex Programming* Society for Industrial and Applied Mathematics.

[34] Boyd, S., and Vandenberghe, L., 2004, *Convex optimization* Cambridge university press.

[35] Verhoeven, R., 2004, "Analysis of the workspace of tendon-based stewart platforms," PhD thesis, Universität Duisburg-Essen.

[36] Jorge Nocedal, S. J. W., 2006, *Numerical Optimization* Springer New York, NY.

[37] C. Masone, H. H. B., and Stegagno, P., 2016, "Cooperative transportation of a payload using quadrotors: A reconfigurable cable-driven parallel robot," *IEEE/RSJ International Conference on Intelligent Robots and Systems (IROS)*.

[38] Métillon, M., Charron, C., Subrin, K., and Caro, S., 2022, "Performance and interaction quality variations of a collaborative cable-driven parallel robot," *Mechatronics*.

[39] Paola, V. D., Ida, E., Zoppi, M., and Caro, S., 2022, "A preliminary study of factors influencing the stiffness of aerial cable towed systems," *ROMANSY, Springer International Publishing*.